Chemical Geology
October 2023, Volume 636, Pages 121652 (12p.)
https://doi.org/10.1016/j.chemgeo.2023.121652 https://archimer.ifremer.fr/doc/00849/96068/

Mercury deposition in the Eastern Mediterranean: Modern fluxes in the water column and Holocene accumulation rates in abyssal sediment

Cossa Daniel [1, 2, *], Guédron S. [1], Coquery Marina [3], Calafat A. [4], Zuñiga D. [4], Stavrakakis S. [5], Radakovitch O. [6, 7], Buscail R. [8], García-Orellana J. [9], Heussner S. [8]

[1] Univ. Grenoble Alpes, Univ. Savoie Mont Blanc, CNRS, IRD, IFSTTAR, ISTerre, 38000 Grenoble, France
[2] IFREMER, Atlantic Center, LBCM, 44031 Nantes, France
[3] INRAE, UR RiverLy, 5 rue de la Doua CS 20244, 69625 Villeurbanne, France
[4] GRC Geociències Marines, Departament de Dinàmica de la Terra i de l'Oceà, Facultat de Ciències de la Terra, Universitat de Barcelona, Barcelona 08028, Spain
[5] Hellenic Center for Marine Research, Institute of Oceanography, 19013 Anavyssos, Greece
[6] Aix Marseille Université, CNRS, IRD, INRAE, Coll France, CEREGE, 13545 Aix-en-Provence, France
[7] IRSN (Institut de Radioprotection et de Sûreté Nucléaire), PSE-ENV/SRTE/LRTA, 13115 Saint-Paul-lès-Durance, France
[8] Univeristé de Perpignan Via Domitia, CEFREM, UMR 5110, 66860 Perpignan Cedex, France
[9] Departament de Física-ICTA, Universitat Autònoma de Barcelona, 8193 Bellaterra, Spain

* Corresponding author : Daniel Cossa, email address : dcossa@ifremer.fr

Abstract :

Modern and past mercury (Hg) fluxes in the oceanic water column and abyssal sediments are poorly quantified. Here, we investigated the particulate transfer of Hg in the water column of the ultra-oligotrophic Ionian Sea (Eastern Mediterranean) with sediment traps during a one-year period, and its accumulation in the deep central abyssal plain using sediment cores comprising the last 10 ka. The Hg concentrations in the particles collected in the sediment traps varied from 112 to 401 ng g−1 and enabled quantifying annual Hg fluxes of 2.0, 2.5, and 2.5 μg m−2 a−1, for traps deployed at 250, 1440, and 2820 m deep, respectively. Hg collected in the upper trap originates from atmospheric deposition, including Saharan dust, which is scavenged by the biological pump. Higher Hg fluxes found at mid-depth and near-bottom than in the upper water layer are attributed to lateral advection under the mixed layer of Hg-rich resuspended sediments from the Adriatic continental margin. In the abyssal sediment, Hg concentrations range from 15 to 134 ng g−1 with the highest levels in the Sapropel S1. Methylmercury concentrations varied from 0.06 to 0.24 ng g−1 following the distribution of total Hg, with evidence of its specific accumulation at the oxidized front of the sapropel. We estimated that <1.8% of the total Hg in the sedimentary column was diagenetically reallocated. The reconstruction of historical Hg accumulation rates (HgAR) during the Holocene shows low pre-anthropogenic values (~0.3 μg m2 a−1 before 4 ka BP), increasing up to ~0.9 μg m2 a−1 during the late Iron Age and the Roman period (1.5–2.5 ka BP), and up to 2.9 μg m2 a−1 during the Industrial Era. During the Sapropel S1 period (~6–10 ka BP), HgARs rose to 6.4 μg m−2 a−1 likely due to the intensity of the Hg removal by the biological pump, the organic matter

preservation, along with high inputs of Hg-rich terrigenous matter and a possible restricted recycling in the atmosphere. Hg accumulation in the Ionian Sea deep sediment is found ~3-fold lower than those in the western Mediterranean abyssal plain.

Highlights

► Mercury (Hg) was studied in water column particles and sediments of the Ionian Sea. ► Average Hg fluxes through the water column varied between 2.0 and 2.5 μg m^{-2} a^{-1}. ► Sediment Hg accumulation rates (HgAR) for the Industrial Era was 2.9 μg m^{-2} a^{-1}. ► HgAR in sediment has increased 3-fold in the last 4 ka. ► Before 6000 years ago in the Sapropel S1, the Hg AR reached up to 6.4 μg m^{-2} a^{-1}.

Keywords : mercury, Mediterranean, flux, accumulation rates, sediment traps, sediment core

1. Introduction

The mercury (Hg) transfer and accumulation in deep-sea sediments are still poorly quantified (e.g., Outridge et al., 2018; Hayes et al., 2021). Estimates of Hg fluxes associated with oceanic settling particles vary by more than one order of magnitude from 0.3 to 4.6 µg m^{-2} a^{-1} (Munson et al., 2015; Cossa et al. 2021), and the global deep-sea Hg annual burial estimations fluctuate by a factor of 7 from 220 to 1540 Mg (Amos et al., 2014; Zhang et al., 2015; Outridge et al., 2018; Hayes et al., 2021). This is explained by the large variability of the few published measurements on Hg concentrations in sediment

trap material, and abyssal sediments (e.g., Gobeil et al., 1999; Ogrinc et al., 2007; Gehrke et al., 2009; Munson et al., 2015; Cossa et al., 2021). The high Hg contents and accumulation rates found recently for hadal sediments reinforce the need for more work on deep-ocean Hg fluxes to better constrain global Hg models (Sanei et al., 2021). It is, therefore, necessary to acquire new Hg measurements and further estimate the flux of sinking particles down to the deep-sea floor from different oceanographic regions presenting biogeochemical contexts as diverse as possible.

Several approaches can be used to estimate the Hg transfer and accumulation rate (HgAR): multiplying Hg concentrations in a given layer of sediment or in particles collected in a sediment trap (Rutten et al., 2000; Outridge et al., 2007; Lim et al., 2017; Aksentov et al., 2021), by sedimentation rates (SR), whilst taking into account porosity and density of the sediments; alternatively, it is feasible to access HgAR by normalizing Hg sediment concentrations to the concentration of a tracer with a known vertical flux, such as ^{230}Th (e.g., Bacon, 1984). Hayes et al. (2021) assert that the ^{230}Th approach has the advantage of not being affected by age model error and by post-depositional redistribution of the sediments. Indeed, the first approaches (i.e., Hg concentration multiplied by SR) are only seemingly simple. Although post-depositional mobility of Hg in sediments is small, it is not completely negligible (Gobeil and Cossa, 1993; Mercone et al., 1999; Rydberg et al., 2008; Gehrke et al., 2009; Cossa et al., 2021). On the other hand, the journey of particulate Hg through the ocean water column down to the sediments is accompanied by homogenous and heterogenous chemical transformations (e.g., Lamborg et al., 2016). The efficiency of the vertical transfer of Hg to sediments is governed by plankton productivity and its uptake rate (i.e., the intensity of the biological pump) and by the aggregation of biogenic particles together and with lithogenic material (Mason et al., 2012; Lamborg et al. 2014; Munson et al., 2015; Zaferani et al., 2018; Jiskra et al., 2021). Indeed, Hg incorporation and accumulation into settling particles depend on the scavenging capacity of the carrier phase (particulate organic matter (POM) including plankton, detrital or authigenic material), and, *a contrario,* on the ability of Hg remobilization during the solubilization-mineralization of the settling POM, occurring particularly *via* Hg methylation or reduction during the downward export of settling material. As reported above, field measurements have shown that the intensity and

composition of the downward Hg fluxes are highly variable depending on the water depth, the geographical location, and the season. In the open ocean, Hg particulate fluxes originate mainly from atmospheric deposition, including aerosol deposition and gas exchange, whereas, in areas closer to the margins or ridges, lateral advection of material from shelves and hydrothermal sources constitutes additional sources (e.g., Fitzgerald et al., 2007; Mason et al., 2012). Atmospheric dust deposition upon oceans is patchy and gas exchanges at the sea surface are highly dependent on the existing physical conditions. Hydrothermal inputs are rare and very localized. In that context, several questions concerning the scavenging and accumulation rates of Hg in open ocean sediments remain open to discussion. Among them: (i) what are the Hg sources, (ii) what are the variations of the downward Hg flux in the water column, (iii) what is the time trend of the HgAR over millennia, and (iv) which proportion of Hg is involved in methylation/demethylation processes and diagenetic rearrangement after its incorporation into sediments?

Here, we present the results of Hg distribution in particles collected in sediment traps during a one-year period and in ~30 cm long sediment cores from a central deep location of the ultra-oligotrophic Ionian Sea (eastern Mediterranean). This allowed us to explore the Hg deposition during the Holocene and its possible mobility associated with the presence of the well-known S1 sapropel (e.g., De Lange et al., 1989). This article is a companion paper to an analogous study carried out in the Balearic basin of the western Mediterranean Sea (Cossa et al., 2021), which provided a Late Holocene reconstruction of HgARs.

2. General settings of the Ionian Sea sediments

The pelagic eastern Mediterranean Sea is ultra-oligotrophic with a low sedimentation rate (SR) averaging between ~2 and 4 cm ka^{-1} (e.g., Thomson et al.; 1995; Garcia-Orellana et al., 2009; The MerMex Group, 2011). In the Ionian Sea, SRs have remained constant for at least the last past 1000 years (Castagnoli et al., 1990). The principal contributors to sedimentation are eolian deposition mainly from Sahara dust, and autochthonous organic matter, including biogenic carbonates, whereas continental inputs from coastal erosion and rivers are low (e.g., Guerzoni et al., 1997; Rutten et al., 2000). However, mud

volcanoes are common structures in the eastern Mediterranean but are mostly located along the Mediterranean ridge (e.g., Nikitas et al., 2021). Recent surficial sediments (~1.5 cm) are well-oxygenated and bio-mixed (e.g., Pruysers et al., 1991; Ogrinc et al., 2007; Angelidis et al., 2011). In contrast, older and deeper sediments are composed of alternating sequences of organic-poor (<0.3% organic carbon) hemipelagic sediments and organic-rich (from 0.5 to 30% organic carbon) sapropelic layers (De Lange et al., 1989; Calvert et al., 1992; Bouloubassi et al., 1999). These alternations result from sharp changes in the photic layer productivity and redox conditions during sediment deposition, such as the sapropel dated to the transition between the Holocene and the Pleistocene (Gehrke et al., 2009; The MerMex Group, 2011).

3. Material and methods

3.1. Samplings

Sediment trap moorings and collections and sediment corings have been performed in April 2001, October 2001, and April 2002 during the ADIOS cruises conducted in the Ionian basin. Automated sediment traps (Technicap® cylindrical traps, Heussner et al., 1990) with a 0.125 m^2 collecting area were deployed at Sta. EB in the Ionian Sea (Fig. 1). Three sediment traps with 12 collection cups were set at each line at nominal depths of 250 m and 1440 m below the surface, and 2820 m (25 m above the sea bottom). The samples were collected every two weeks for more than 11 months from the 1st of May 2001 to the 15th of April 2002. A total of 69 samples were collected for the elementary analyses. However, when the amount of material was insufficient for the analysis, samples were sometimes pooled resulting in 28 samples for Hg analyses. The samples were frozen immediately upon recovery, then freeze-dried, homogenized, and sub-sampled for various subsequent chemical analyses. An undisturbed 30 cm-long box core was obtained from Sta. EA in the Ionian Basin of the Eastern Mediterranean in April 2001, 25 km away from Sta. EB (Fig. 1). The core has been sliced at 0.5 cm intervals over the first 5 cm, at 1 cm intervals from 5 to 20 cm, and at 2 cm intervals from 20 cm to the bottom, on board immediately after recovery. An additional shorter box core was also obtained at Sta. EB, and was sliced only down to 15 cm.

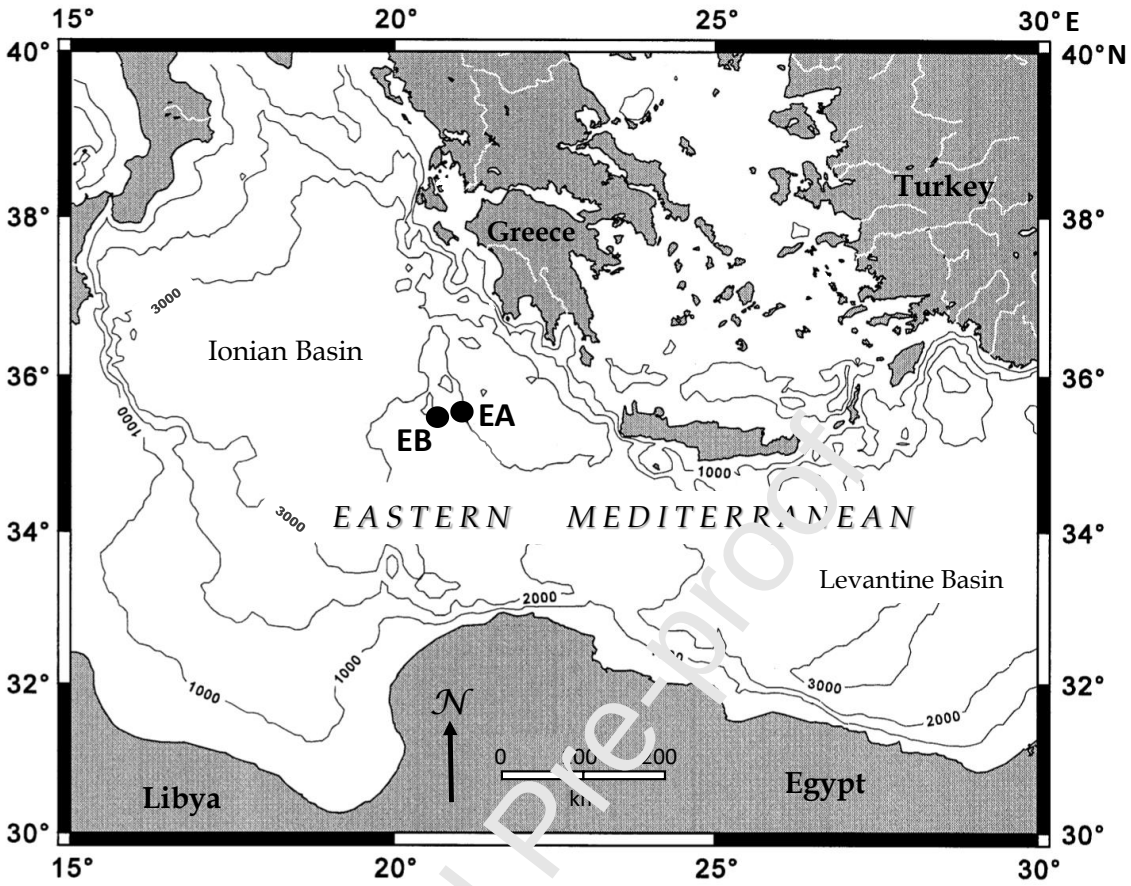

Figure 1. *Locations of the sampling stations in the Ionian Sea. EA (Lat.: 35°04.08'N; Long.: 2°50.94'E): coring; EB (Lat.: 35°04.07'N; Long.: 2°30.49'E): sediment traps mooring. See Suppl. Fig. SI.1 for the meteorological conditions and Saharan dust distribution prevailing during the sampling cruise.*

3.2. Analyses and accumulation rate calculations

Total Hg analyses were performed using an automatic atomic absorption spectrophotometer (Altec®, model AMA-254), according to the protocol described by EPA (2007). Briefly, weighed aliquots of freeze-dried sediment were introduced into the analytical system where they were heated to 550°C. The volatilized Hg was carried by a stream of oxygen to a gold trap onto which Hg was concentrated by amalgamation, before being thermally dissociated and analyzed by atomic absorption spectrometry. The detection limit (DL) was 7 ng g^{-1}, calculated as 3.3 times the standard deviation of the blanks. We used the MESS-2 marine sediment certified reference material (CRM) from the National Research Council of Canada to ensure the accuracy of the analyses; the mean value obtained (92 ± 2 ng g^{-1}) was always within the range of the certified value: 92

± 9 ng g^{-1}. The reproducibility, defined as the coefficient of variation of six replicate analyses of the same CRM was 2%, whereas the analytical uncertainty (Eurachem/Citac, 2000) is ~10%. Labile Hg concentrations were estimated upon partial dissolution of the sediment with diluted HCl (0.5 M) solution according to the protocol described by Kostka and Luther (1994).

Methylmercury (MeHg) concentrations were determined using a method adapted from Leermakers et al. (2001). MeHg was solubilized in 4 M HNO_3 from a freeze-dried sediment aliquot, then extracted by CH_2Cl_2 and transferred into demineralized water by evaporation of the organic solvent. MeHg in the water phase was then ethylated and purged on a Tenax-packed column. The ethylmethylmercury formed was isolated from other volatile compounds by gas chromatography and quantified by cold vapor atomic fluorescence spectroscopy. The DL (DL = 3.3 times the sd of blank values) was 0.003 ng g^{-1}. The analytical precision, determined from replicate analyses (n = 6), was <15%. Recoveries of MeHg in the CRM 405 material from the International Atomic Energy Agency (IAEA) were 91 ± 8% (n = 6).

Total organic carbon (C_{org}) content and its isotopic composition ($\delta^{13}C_{org}$) were measured on freeze-dried and homogenized subsamples after decarbonatation. Total carbon (C_t) and nitrogen (N_t) were determined with an elemental analyzer (Model CN 2000, LECO®) after acidification with 2 M HCl (overnight, at 50°C. The precision (6 replicates of a sample) for C_{org} and C_t analyses was 0.1%, and 0.3 % for N_{org}. Concentrations are expressed as the weight percent of dry matter. Calcium carbonate content was calculated from mineral carbon (C_t- C_{org}) using the molecular mass ratio $CaCO_3$:C = 100:12. Stable isotopes have been on a Flash 1112 EA elemental analyzer interfaced to a Delta C Finnigan® MAT isotope ratio mass spectrometer. Uncertainty was lower than 0.05‰.

Major elements were analyzed by X-ray fluorescence spectrometry and results were published earlier (Angelidis et al., 2011). Labile Fe (and associated Hg) concentrations were estimated upon partial dissolution of the sediment with dilute HCl (0.5 M) solutions according to protocols described by Kostka and Luther (1994). The HCl extraction

dissolves carbonates, crystalline Fe-oxyhydroxides, and acid-volatile sulfides. It should be noted that the 0.5 M HCl extraction does not dissolve HgS (Mikac et al., 2000).

HgARs were computed with consideration of the sediment compaction, as performed previously for the western Mediterranean Sea (Cossa et al., 2021), following the equation:

$$HgARs = 10*[THg]*SR*(1-\varphi)*d \quad (1)$$

where [THg] is the Hg concentration (ng g^{-1}), SR the sedimentation rate (cm yr^{-1}), φ the porosity of the sediment (Suppl. Table S1), and d the average dry bulk sediment density, 2.65 g cm^{-3} according to Hamilton (1976).

4. Results

4.1. Sediment trap material

Microscopic examination and X-Ray diffraction (XRD) analysis of the material collected in the traps revealed the presence of fecal pellets and planktonic organisms with the dominance of foraminifera and pteropod species embedded in an amorphous organic and lithogenic material. The details of these observations are given in the ADIOS final report (ADIOS, 2004) and all the analytical results are presented in Suppl. Table SI.2. The lithogenic fraction was prevailing in terms of mass (i.e., 40 to 77%, Fig. 2A). Biogenic carbonates constituted the second major component of the collected material in the traps (i.e., 11 to 59%, Fig. 2C) and their distribution over time mirrors the lithogenic fraction. None of these fractions showed statistically significant differences with depth (Table 1). C_{org} increases from 2% at the beginning (April 2001) to 10% at the end of the experiment (March 2002), with a marked drop in winter more than likely as a result of the low productivity in the mixed layer at this season (Fig. 2B). The annual mean C_{org} concentration at 250 m was twice ($p<0.01$) the ones at other depths except during winter. This is illustrative of the dynamic of biological production in the mixed layer and of the remineralization process below. The $\delta^{13}C_{org}$ ranged between –22.2‰ and –24.5‰, and the $\delta^{15}N$ signature between +0.9 ‰ and +3.9 ‰ (Suppl. Table SI.3). These tracers varied in-mirror, with $\delta^{13}C_{org}$ decreasing and $\delta^{15}N$ increasing, during summer and autumn at

depth suggesting an enhancing contribution of terrigenous organic material (Suppl. Fig. SI.2). The settling particle total mass flux (Fig. 2D) peaked during the spring (i.e., April 2001 and March 2002) with 10 to 20 times higher fluxes than the autumn and winter baseline values. The total mass flux during the entire collection period for the site EB was the lowest at 250 m (15 g m^{-2} d^{-1}), compared to 27 and 23 g m^{-2} d^{-1} at 1440, and 2820 m, respectively (ADIOS, 2004).

Table 1. *Mean concentrations (±1SD) of the main components of the particles collected twice a month in the traps between May 2001 and April 2002 at Sta. EB. * Mean concentration significantly ($p<0.01$) different from means at 1440 and 2820 m); other differences are non-significant.*

Depth (m)	Lithogenic (%)	Carbonates (%)	C_{org} (%)	Hg_S (ng g^{-1})	Hg/C_{org} (molar ratio 10^{-6})
250	58.9 ± 12.9	31.7 ± 13.7	6.3* ± 2.5	265 ± 68	0.29* ± 0.13
1440	54.2 ± 8.0	39.3 ± 6.2	3.3 ± 1.7	236 ± 69	0.45 ± 0.12
2820	58.5 ± 9.7	35.1 ± 9.6	3.2 ± 1.1	248 ± 82	0.49 ± 0.19

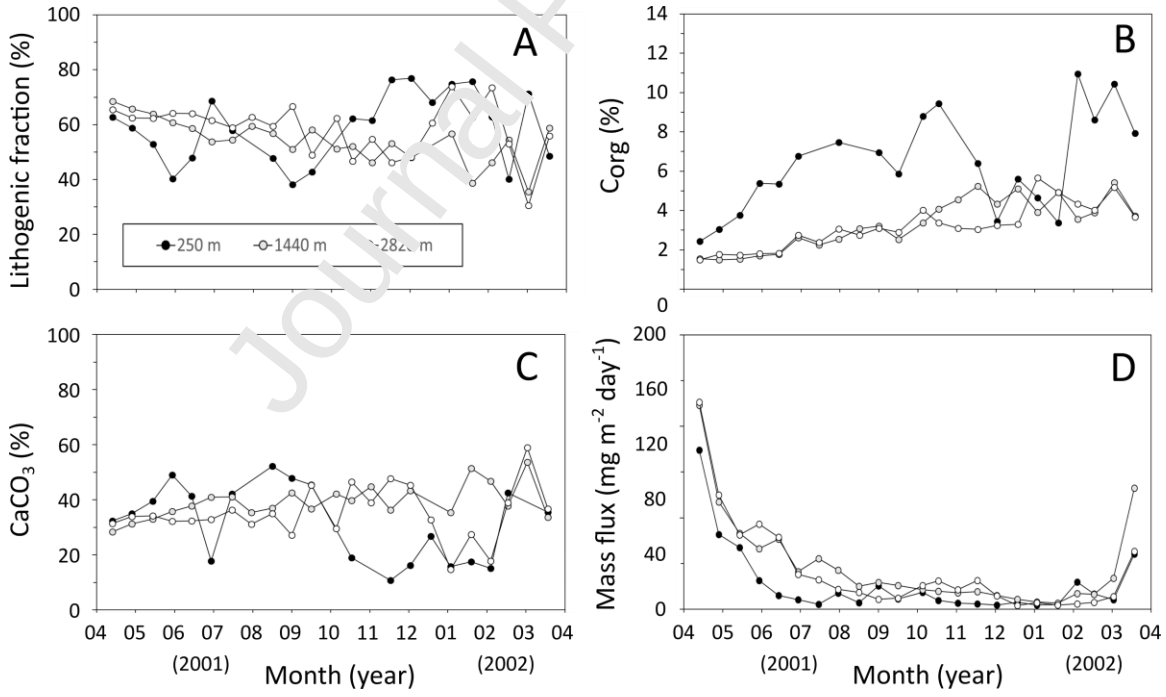

Figure 2. *(A) Lithogenic fraction, (B) organic carbon, (C) carbonates, and (D) mass flux during the year 2001-2002 in the three sediment traps at Sta. EB. Saharan dust events were mainly observed in spring.*

Hg concentrations measured in the trapped particles varied from 112 to 401 ng g^{-1}, with an overall mean Hg concentration of 250 ± 73 ng g^{-1}. Mean Hg concentrations for the entire sampling period did not differ significantly with depth (*t*-tests, *p>0.10*, Table 1). In contrast, concentrations differed over time with significantly lower values in the spring compared to other seasons (Fig. 3A). In particular, at 1440 and 2820 m, mean Hg concentrations were two-fold lower in spring compared to autumn (134 ± 23 ng g^{-1} *versus* 310 ± 73 ng g^{-1}, *p<0.01*, *t*-test). Interesting to note is the occurrence of high Hg concentrations in autumn when $\delta^{15}N$ and $\delta^{13}C_{org}$ values testify to the enhanced presence of terrestrial material. Despite the seasonal variation of Hg concentrations, Hg fluxes follow the total mass fluxes with the highest vertical transport in spring (Fig. 2D). The integrated Hg fluxes, calculated for the period May 2001 to April 2002, were 2.0 ± 0.8, 2.5 ± 0.7, and 2.5 ± 0.9 µg m^{-2} a^{-1}, at 250, 1440, and 2820 m, respectively.

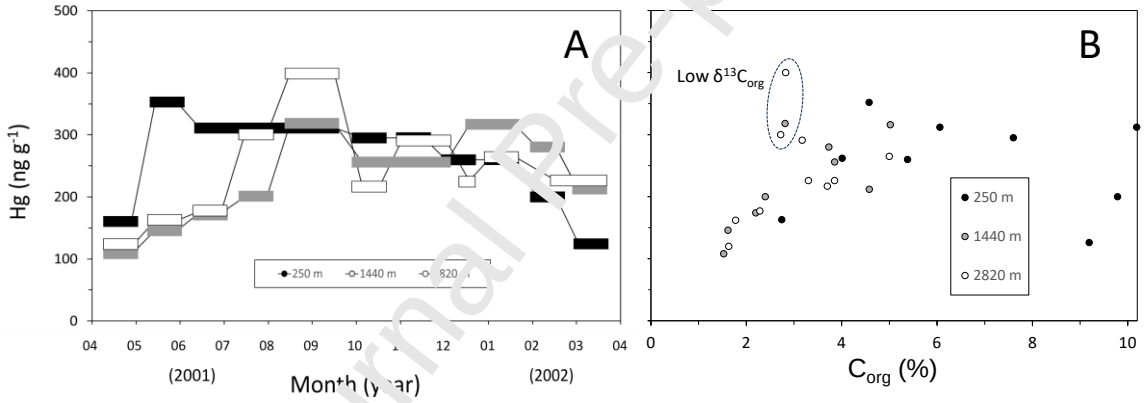

Figure 3. *(A) Hg concentration in the particulate material collected during the year 2001-2002 in the three sediment traps at Sta. EB. Low Hg concentrations are observed in spring; (B) Hg vs organic carbon (C_{org}) in particulate material collected during the year 2001-2002 in the three sediment traps at Sta. EB. Low $\delta^{13}C$ values, suggesting terrigenous OM, are associated with Hg-rich particles. C_{org} > 5% values may involve a bio-dilution of particulate Hg*

4.2. Sediment core material

Core EA consists of light brown calcareous pelitic muddy sediments from surface to 18 cm. Below, a dark layer down to 24 cm corresponds to the level where Sapropel S1 has already been identified in the Eastern Mediterranean (e.g., De Lange et al., 1989; Thomson et al., 1995; Murat & Got, 2000). Core EB was similar but shorter and did not include the sapropel layer. C_{org} concentrations (Fig. 4A, insert) were < 0.5% in most of the cores decreasing from the surface to 10 cm below (from ~0.5 to ~0.2%) in both cores.

However, below 18 cm in core EA, C_{org} increased sharply to peak (2.6%) at 21.5 cm, testifying of the sapropel layer, which is confirmed by the highest concentration of Ba/Al, a paleoproductivity indicator, between 20 and 25 cm (Fig. 4B). The distributions Mn/Al and Mo/Al ratios(Fig. 4C) were typical of redox-sensitive elements. They exhibit well-defined peaks above the sapropel (~15-17 cm) indicating the oxidation front of the sapropel, consistent with patterns reported for the Sapropel S1 in a nearby station of the same basin (Filippidi and De Lange, 2019).

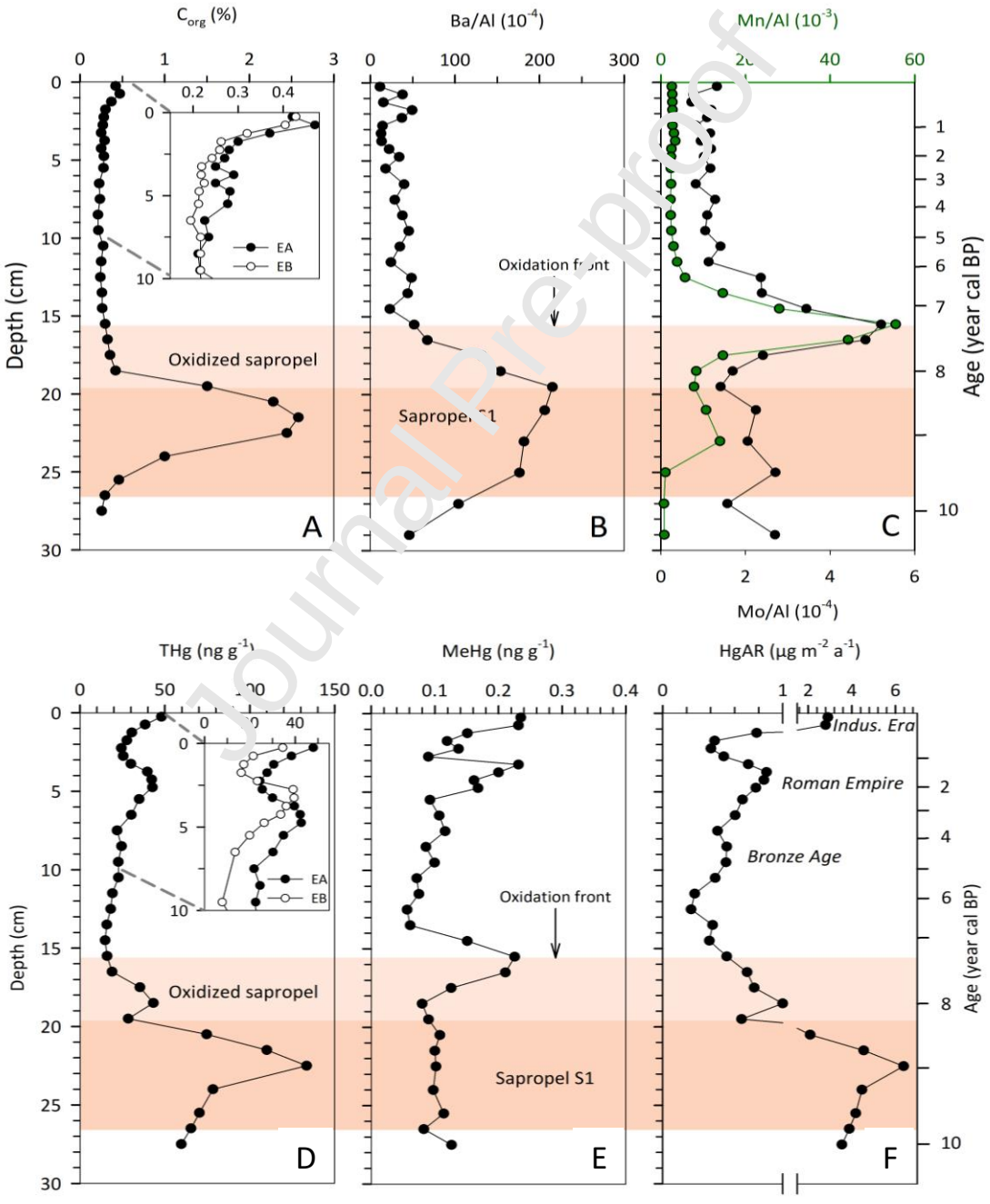

Figure 4*. Vertical distributions of C_{org} (A), Ba/Al (B), Mn/Al with Mo/Al (C), Hg (D), MeHg (C), and HgAR (F) in sediment cores EA and EB. The onset, ending, and oxidized part of the sapropel S1 are indicated (see text). The oxidized front is defined by the presence of Mn/Al and Mo/Al peaks.*

Hg concentrations in cores EA and EB ranged from 15 ng g^{-1} to 134 ng g^{-1} (Fig. 4D). Vertical profiles of Hg concentrations are characterized by smooth variations including (i) a decrease between 0 and 2 cm, then (ii) a bump between 2 and 7 cm, and (iii) low concentrations down to 10 cm. In addition, two Hg peaks were associated with the sapropel layer in core EA: the main Hg peak (between 21 and 23 cm) coincidental with the maximum of C_{org} (Fig. 4A), and the secondary peak (18.5 cm) in the oxidized part of the sapropel (Fig. 4D). It is important to note that the normal zero relations of Hg/Al or Hg/Si exhibit similar profiles as the Hg concentration (Suppl. Fig. SI.3), which demonstrates that the Hg variations are not due to changes in the lithology of the sediments. The MeHg measured in the EA core (0.06 to 0.24 ng g^{-1}) represents on average 0.4% of the total Hg. Its vertical distribution (Fig. 4E) exhibits 3 peaks; one at the surface, the second between 3 and 5 cm, and the third between 14 and 17 cm. The first two peaks of the MeHg distribution are coincidental with total Hg peaks (Fig. 3A and B).

5. Discussion

5.1. Sources of particles and associated Hg in the trapped material

Particulate matter collected in the sediment traps at station EB is mainly composed of lithogenic particles and biogenic carbonates suggesting the presence of terrestrial material embedded in a biogenic matrix. Vertical mass fluxes reach their maximum in spring whatever the depth, but are higher in the deep traps compared to the upper one. This pattern supports major particulate mass fluxes during the biological productive period and lateral advection below the mixed layer (Fig. 2). In contrast, the OM fraction is higher in the upper trap material compared to deeper ones except during winter when the biological production collapses.

The composition of the lithogenic material is dominated by quartz, clay minerals, and feldspars (ADIOS, 2004), indicating various sources including the advection of river

particles, coastal erosion, resuspension of sediments, and Saharan dust deposition. Indeed, Adriatic sediments are composed of sand, silt, and clay, including significant fractions of quartz, calcareous material, feldspars, and OM (Faganeli et al 1994; Droghini et al., 2019). On the other hand, according to Kandler et al. (2007), the composition of the Saharan dust particles is dominated by phyllosilicates, with significant fractions of quartz, and carbonaceous material. Although the expected increase in kaolinite during Saharan dust events was not ascertained, 40% of our sampling period consisted of dusty days and Saharan dust events have been registered in the spring of 2001 (Suppl. Fig. SI.1; Georgopoulos et al., 2002; ADIOS 2004). The presence of biogenic carbonates formation in the mixed layer at station EB is attested by the temporal covariation of $CaCO_3$ and C_{org} content of the material collected in the trap at 250 m (Fig. 2B and C). Our results are consistent with previous observations showing that biogenic carbonates constitute a major part of the phytoplankton production and carbonate flux between February and June in the Ionian Sea (Moulin et al., 1998; Powley et al., 2017; Skampa et al., 2020; Pedrosa-Pamies et al., 2021). Such an increase in primary production has been shown to be triggered by the nutrient enrichment of surface water resulting from Saharan dust deposition (e.g., Gallisai et al., 2014; Pedrosa-Pamies et al., 2016). Thus, the seasonality of the mass flux appears to be governed by variations in phytoplankton production in the photic zone and Saharan dust deposition in a process similar to that described for the Northwestern Mediterranean wherein the downward particulate flux is modulated by the lithogenic contribution to settling particles ballasting the biogenic material (Ternon et al., 2010). The isotopic compositions of C and N allow us to identify the origin of the trapped POM. The highest $\delta^{13}C_{org}$ values found in spring indicate a marine origin of the POM, attributable to phytoplanktonic production in the euphotic layer. In May 2001, the $\delta^{13}C_{org}$ and $\delta^{15}N$ values of sinking settling POM were very similar and covaried at 250 m, 1440 m, and 2820 m, supporting a top-down control of the organic fraction flux, from the euphotic zone to the bottom. In contrast, at the end of the summer and the beginning of autumn, lower $\delta^{13}C_{org}$ and higher $\delta^{15}N$ values of POM collected in the intermediate and deeper traps than at 250 m supports increased inputs of terrigenous material below the mixed layer.

The involvement of the Hg vertical transfer in the water column with the POM dynamic (biological pump and the terrigenous advection) is illustrated in Figure 3B. When C_{org} is < 5%, the positive covariation between the Hg and C_{org} (R^2 = 0.39, *p<0.05*) suggests that POM plays a major role in the vertical transfer of Hg to the bottom sediments. This positive relationship is even much stronger (R^2 = 0.73, *p<0.01*) when values of the terrigenous samples (with low $\delta^{13}C_{org}$ values) collected at the end of summer and the beginning of autumn at 1440 and 2820 m are removed from the calculation. When C_{org} concentrations are > 5%, i.e., during the productive period of early spring 2002 (Fig. 2B), Hg concentrations do not increase with C_{org} (Fig. 3B), suggesting that the Hg available for the biological pump has been exhausted from the mixed layer. In other words, this pattern would result from the biodilution of the Hg pool of the euphotic zone during phytoplanktonic efflorescence. Besides, we assume that most of the lateral inputs of particulate matter to the EB site originate from the resuspension of Adriatic sediment with a substantial terrigenous origin (Manca et al., 2002) conveyed to the interior of the Ionian Sea by convective currents (e.g., Berline et al., 2021; Pedrosa-Pamies et al., 2021). Thus, the Hg concentrations of the Adriatic surface sediments should determine the magnitude of the Hg advected with this process. Hg concentrations in Adriatic sediments vary widely from ~50 ng g^{-1} for matter originating from the Southern part of the Adriatic to > 1000 ng g^{-1} for that originating from its Northern part (Droghini et al., 2019). The presence of anthropogenic Hg in the Northern Adriatic sediments has been evidenced and ascribed to mining activities and direct industrial inputs (e.g., Kotnik et al., 2015). Combining these observations, it can be inferred that the high C_{org}, low $\delta^{13}C_{org}$ and high Hg content (> 250 ng g^{-1}) of the settling material collected at depth in autumn at the EB site reflect the advection of Hg-enriched POM originating from the resuspension of Hg contaminated sediments likely from the Northern Adriatic. On the other hand, the Hg concentrations in the Saharan dust are less constrained than those of the Adriatic sediments. The few Hg concentrations available for the Saharan dust aerosols measured at the Cape Verde and Canaries Islands (Bailey, 2021) give a mean Hg concentration of 73 ± 7 ng g^{-1} (n=5) for the year 2020. In the spring of 2001, the Eastern Mediterranean atmosphere was characterized by southerlies transporting high quantities of Saharan dust (Georgopoulos et al., 2002; Sciarra et al.,

2004). Moreover, the spring-2001 cruise took place immediately after a cloud of Saharan dust passed over the Ionian region (Suppl. Fig. SI.1). At that time, the local circulation was favorable for dust transport from the surface to the deeper layers, due to the presence of a deep anticyclone. In spring 2001, Hg concentrations collected at the 250 m trap were greater than 150 ng g^{-1}, ruling out the Saharan dust as the main Hg carrier. On the contrary, Saharan dust probably dilutes the Hg-rich biogenic particles. Furthermore, the most probable role of Saharan dust in the Hg transport to the bottom is a ballasting effect upon the biological pump. The contribution of Hg deposition associated with Saharan dust can be independently assessed based on the most recent estimates of the total mass deposition rates of Saharan dust onto the eastern Mediterranean basin (7.4 g m^{-2} a^{-1} according to Vincent et al., 2016) and the only available mean Hg concentration in the Saharan aerosols (73 ng g^{-1} according to Bailey, 2021). In these conditions, the mean contribution of particulate Hg fluxes from the Sahara is ~0.52 µg m^{-2} a^{-1} and represents one-fifth of the total Hg collected in the traps. However, this estimate is fraught with great uncertainty, since Hg concentrations in Saharan dust are still weakly documented and the total mass deposition rates of Saharan dust on the Ionian Sea are poorly constrained, ranging from 1 to 50 g m^{-2} a^{-1} (Guerzoni et al., 1999; ADIOS, 2004; Guieu and Shevchenko, 2015; Vincent et al., 2016).

5.2. Sources and accumulation of Hg in sediment above the sapropel

Recently, Friedling et al. (2023) concluded that high amplitude oxygen fluctuations in the water column and shallow sediment may lead to increased variability in Hg and OM buried in sediments. Indeed, according to these authors, under oxygen depletion conditions, a part of Hg can escape from sediments after methylation and reduction. Contrarily, aerobic degradation would affect the sedimentary OM, whereas Hg would be mainly retained in the sediment. In order to explore the possible Hg mobility associated with redox changes we proceeded to an estimation of the Hg species solubilized with dilute HCl (here called “mobile Hg fraction”), which is supposed to dissolve amorphous oxy(hydr)oxides and sulfides (Kostka and Luther, 1994). The mobile Hg fraction, which constitutes < 1.8% of the total Hg (Suppl. Fig. SI.5), presents a vertical distribution in surface sediment indicating that the vertical Hg distribution within this layer is mainly governed by external input and the relative proportion of various carrier phases.

Consistently, the first 15 cm sediment of the core EA (i.e., above the S1 sapropel) is an oxic layer without any trace of change of redox conditions, which would make a possible reallocation of the Hg in the sedimentary column; thus, the possible involvement of Hg in diagenetic homo- and heterogeneous reactions is very unlikely.

As discussed for the particulate Hg flux through the water column, the main carrier which conveys Hg to the sediment is POM from planktonic production and terrestrial detritus inputs. First, the biological pumping, initiated by phytoplankton production, scavenges Hg from atmospheric deposition. Second, the advection of coastal material enriched or not with Hg from coastal regions has been identified in sediment traps. In addition, in the Ionian Sea, the role of volcanic and hydrothermal inputs must be taken into account. The contribution of the biological pump in bringing Hg to the sediments can be explored using the Hg/C_{org} ratios (Suppl. Fig. SI.6A). As in the trapped particles, the Hg is significantly correlated with C_{org} in deposited sediments, but under certain conditions. In Cores EA and EB the overall relationship is highly significant ($R^2 = 0.59$, *$p<0.01$*), but mostly driven by the sapropel content, since above it the R^2 is only 0.26 (*$p<0.10$*) (Suppl. Fig. SI.6B). In these parts of the cores (above the sapropel), the $Hg:C_{org}$ molar ratios varied from 0.32 to $1.01*10^{-6}$ and from 0.30 to $1.08*10^{-6}$ for the EA and EB, respectively (Suppl. Fig. SI6A). In the redox conditions of the EA station, the aerobic degradation of the Hg-OM appears to raise the $Hg:C_{org}$ atomic ratios as illustrated by the difference between the sediment trap material collected at 25 mab (0.49) and the surface of the cores (0.68). These differences suggest that during the OM consumption below the mixed layer, the Hg initially bound to the POM and released upon its solubilization or remineralization must be re-bounded to the residual settling particles and that this process occurs mostly in the water column near the bottom. If this process was continuing in the sediments we should observe an increase of the $Hg:C_{org}$ ratio with depth which is not the case (Fig. SI.6A). There, time variations of HgAR should be the driving factor.

Besides, it has been suggested that a part of Hg concentration within the first 5 cm below the interface in Ionian Sea sediments originates from the deposition of volcanic ashes (Ogrinc et al., 2019); this hypothesis was based on the changes of $\delta^{202}Hg$ within this layer. However, the $\delta^{202}Hg$ values are very variable Italian volcanic emissions (-1.74

to – 0.11‰ according to Zambardi et al., 2009), and more data are needed to accurately identify the trace of Hg from a volcanic origin in the deep Mediterranean sediments.

5.3. Evidence for Hg relocalization in the S1 sapropel

In the sediment core EA, sapropel S1 is characterized by high C_{org} concentrations (Fig. 4A) which result from OM preservation owing to oxygen-depleted conditions in the bottom waters and high primary production in surface water of the Ionian sea (e.g., Filippidi and De Lange, 2019; Murat & Got, 2000). The high primary production behind the formation of S1 is thought to be due to an increased discharge of freshwater into the Mediterranean following a change to a warmer and wetter climate during the African Humid Period (Ariztegui et al., 2000). The use of Ba/Al distribution, as a paleoproductivity indicator (due to the immobility of Ba as barite according to Thomson et al., 1995), gives more precise limits of the sediment layer concerned by the sapropel, namely 18-27 cm (Fig. 4B). The major element composition of the sedimentary column (Suppl. Fig. SI.4) indicates little changes in the source of material within the sapropel, with less biogenic carbonates and a larger lithogenic fraction. This likely results from a larger contribution of terrigenous material from rivers or Saharan dust during the sapropel deposition (Wehausen and Brumsack, 2000; Böttcher et al., 2003).

High Hg concentrations in Mediterranean sapropels have already been shown: (i) in S1 sapropel collected in the Aegean Sea (Mercone et al., 1999), and (ii) in a mi-Pleistocene sapropel collected in the Tyrrhenian basin of the western Mediterranean (Gehrke et al., 2009). According to these authors, this Hg enrichment is due to the intensity of the Hg removal by OM associated with oxygen depletion in the water column. In the case of the mid-Pleistocene Mediterranean sapropel, Gehrke et al. (2009) concluded even that OM quantitatively delivers the Hg present in the mixed layer to the seafloor. Other authors also argued that the high terrigenous fraction of the sapropelic OM may favor its elevated $Hg:C_{org}$ ratio (e.g., Böttcher et al., 2003). In core EA, the $Hg:C_{org}$ atomic ratio was quite variable (Fig. SI.6A) as it is in the settling particles collected at 250 m in the water column (Fig. 3B). These similar situations suggest that during the highly productive period of Sapropel S1, the biological pump was exhausting all the Hg present in the euphotic zone as observed by Gehrke et al. (2009) in the mid-Pleistocene sapropel.

In the oxidized part of the sapropel, a diagenetic mechanism may have induced the development of the secondary Hg peak observed at 18.5 cm depth (Fig. 4D) in the sediment layer defined by the dramatic decrease of Ba/Al and the rise in Mn/Al above (Fig. 4), where barite is dissolved in presence of (trace) sulfides, while Mn starts to precipitate in oxic sediments. This Hg peak should result from the reallocation of a small amount of Hg associated with sapropelic OM. In the Sapropel S1, sampled nearby in the Aegean Sea, Mercone et al. (1999) have already observed sharp Hg peaks in suboxic conditions where sediments containing trace pyrite have been re-oxidized. These authors proposed that such reallocation occurred following the release of Hg into the pore water solution during the reduction of oxide minerals. The Hg is then re-immobilized under reducing conditions associated with pyrite or in the form of HgS and/or HgSe. Here, the hypothesis of Hg incorporation in pyrite is supported by the significant relationship between Hg and Fe in the sapropel layer, i.e., between 16 and 25 cm below the sediment-water interface ($R^2 = 0.58$, n = 9, $p < 0.01$). The mobile Hg fraction (i.e., Hg_{HCl}, Suppl. Fig. SI.5), presents a main peak on the top of the oxidized sapropel coincidental with the Mn/Al and Mo/Al peaks (Fig. 4C). This suggests that a small proportion of Hg was remobilized during oxidation of OM diffusing along the concentration gradient, and readsorbed onto oxy(hydr)oxides (associated or not with remaining POM), as Cu and Zn already analyzed in this core (see figure 3 in Angelidis et al., 2011). As suggested by Mercone et al. (1999): "…[the] redox gradient across the [oxic-suboxic] boundary, imposes thermodynamic controls on elemental speciation, which leads to the development of peaks at slightly different depth levels for different elemental geochemistries". The amounts of relocalized trace elements vary in response to their relative reactivity with OM and adsorptive rate by oxy(hydr)oxides, in the order Cu<Zn<<Hg (Feyte et al., 2010). Angelidis et al. (2011) have noted that, in core EA, the Pb profile (Suppl. Fig. SI.7), contrary to the cases of Cu and Zn, does not show evidence for diagenetic remobilization, and its distribution is governed by external input. During sediment sulfidization, especially in the sapropel layers, the Hg-Fe association would shift from the adsorption onto the oxy(hydr)oxides to the incorporation into sulfides.

5.4. Methylmercury in sediments

MeHg pattern is consistent with the general model showing that the net MeHg abundance in sediments is a function of the inorganic Hg considered as the substrate of enzymatic reactions and that a part of the signal may remain inscribed in the oxic sediments (Cossa et al., 2014). The third MeHg peak is located above the sapropel, while the sapropel itself has low MeHg concentrations, but very high total Hg levels *a contrario* to what occurs in the two MeHg peaks described above (Fig. 4D and E). High MeHg:Hg ratios in sediments are often associated with Hg net methylation in suboxic environments resulting from sulfate or iron-reducing bacteria activities, whereas low MeHg:Hg ratios are associated with net demethylation occurring mostly under anaerobic conditions (e.g., Figueiredo et al., 2018; Bravo and Cosio, 2019; Regnell and Watras, 2019). High MeHg levels at the oxidation front of the sapropel suggest a Hg methylation by sulfate-reducing bacteria at a relict suboxic zone. During its diffusion upward from the oxidizing zone, MeHg appears to be adsorbed onto Mn-oxy(hydr)oxides as suggested by the strong correlation between MeHg and Mn at the oxidation front (Fig. 5) and constitutes most of the mobile Hg fraction at the top of the oxidized sapropel (Suppl. Fig. SI.5). This link between MeHg and Mn-oxy(hydr)oxides should be favored by OM through the formation of stable bidentate complexes as predicted by modeling (Feyte et al., 2010). Below the oxidizing zone, it can be speculated that, if MeHg has been formed in suboxic conditions associated with OM-rich sediment of the sapropel, it has been subsequently demethylated since.

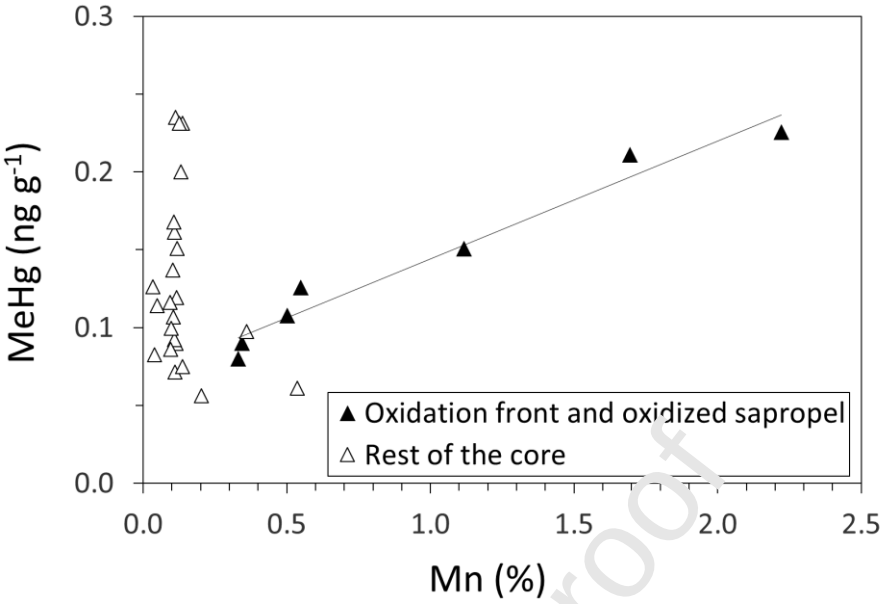

***Figure 5**. Methylmercury (MeHg) and manganese (Mn) relationship in the EA sediments. The oxidation front and oxidized sapropel cover the 14-20 cm sediment layer. In this layer, the MeHg vs Mn relationship exhibits an R^2 of 0.96 ($p<0.01$).*

5.5. Historical reconstruction of Hg accumulation rates in Ionian abyssal sediment

To reconstruct historical Hg fluxes in the Ionian abyssal sediment, a chronological framework was established for core EA (Suppl. Fig. SI.8). An age-depth model was built through the combination of ^{210}Pb activity data and radiocarbon ages of foraminifera (*Universa orbulina*) collected by Garcia-Orellana et al. (2009), at 0-0.5 cm (845 ± 25 a BP), 9-10 cm (4790 ± 50 and 4620 ± 40 a BP), 13-14 cm (6420 ± 35 a BP), and 26-28 cm (11765 ± 50 a BP). The drop of $^{210}Pb_{ex}$ activities and the distribution of other radionuclides (i.e., ^{137}Cs and $^{239+240}$Pu) within the first 1.5 cm in Core EA indicates a mixing of this sediment covering the last past ~120 years (Garcia-Orellana et al., 2009). This is also consistent with the lowest $^{206/207}$Pb values of the EA record (< 1.20, Suppl. Fig. SI.7), which confirms that anthropogenic Pb from the industrial revolution (i.e., since ~100 BP or 1850 CE) is confined in this layer (Angelidis et al., 2011). In addition, the bottom and top of the Sapropel S1 were identified by correlating Ba/Al, Mn/Al, and C_{org} excursions (Fig. 4), and the corresponding ages (Crusius and Thomson, 2003; De Lange et al., 2008; Grant et al., 2016; Rohling et al., 2015; van Kemenade et al., 2023) were used to constrain the age model. Finally, the age-depth model was derived using the IntCal20 calibration curve (Reimer et al., 2020) with consideration of a 390 ± 85 years

marine reservoir age of the Mediterranean Sea (Siani et al., 2000). All details for the construction of the age model are provided in Suppl. Fig. SI.8. Below the 1.5 cm, (i.e., before the Industrial Era), the obtained linear SRs were 2.2 ± 1.0 cm ka^{-1}, in agreement with previously published SRs in that area (e.g., Rutten et al., 2000, De Lange et al., 2008). At the bottom of the core, linear SR increased in the Sapropel S1, up to ~4.3 cm ka^{-1} consistently with reported values for the eastern Mediterranean Sea (De Lange et al., 2008; Filippidi and De Lange, 2019).

The relatively elevated Hg concentrations in the first 1.5 cm below the sediment surface (Fig. 4D) are a common feature in the abyssal sediments of the western Mediterranean (Cossa and Coquery, 2005; Ogrinc et al., 2007; Heimbürger et al., 2012; Cossa et al., 2021). This Hg-enrichment has been attributed to the increased anthropogenic Hg depositions during the Industrial Era, partially bio-mixed within the 1.5 cm surface layer. The resulting Hg accumulation rate (HgAR) calculated for this period is 2.9 µg m^{-2} a^{-1} (Fig. 4F), which is similar to HgAR calculated from the sediment trap near the bottom (~2.5 µg m^{-2} a^{-1}) but about 3 times lower than the values reported for the western basin surficial sediments (~8.9 µg m^{-2} a^{-1}, Fig. 6) (Cossa et al. 2021). It is worth mentioning that these superficial signals, as well as the deeper ones, have been smoothed by a high biological mixing (Garcia-Orellana et al., 2009).

Below the superficial layer, a second Hg bump in concentration between 3 and 7 cm depth corresponds to a rise in HgAR from a baseline of ~0.3 up to ~0.9 µg m^{-2} a^{-1} and centered between 1500 and 1800 BP. A similar observation is made with Pb concentrations, PbARs, and $^{206/207}$Pb profiles (Suppl. Fig. SI.7), and interpreted as the effect of anthropogenic deposition during that period (Angelidis et al., 2011). Such increases in Hg and Pb depositions for the same period have already been reported in a lagoon and the abyssal plain of the western Mediterranean, as well as in Alpine Lake sediments (Elbaz-Poulichet et al., 2011, 2020; Thevenon et al., 2011; Cossa et al., 2021) and attributed to the metallurgic development during the Iron Age and Roman periods. The climate optimum during the Roman Era may have also influenced HgAR, as this period is known as the warmest period of the last 2 ka, being ~ 2°C warmer on average (Margaritelli et al., 2020). This may explain the slight increase in C_{org} observed between 3 and 6 cm in core EA (Fig. 4A insert). However, if such climatic influence may have

influenced HgAR in core EA, it is not the case for core EB where the C_{org} bump around 3-6 cm is not discernable (Fig. 4A, insert), whereas the Hg signal is distinctly present (Fig. 4D, insert). Another slight increase in HgARs (up to 0.53 µg m^{-2} a^{-1}) at ~8 cm depth (Fig. 4F) corresponds to the Bronze Age, a period marked by increased Hg depositions in certain Alpine lake records attributed to local mining activities (Elbaz-Poulichet et al., 2020). Finally, during the Sapropel S1 period (i.e., ~ 5.7 to 9.3 ka cal BP), the HgAR has reached up to 6.4 µg m^{-2} a^{-1} (Fig. 4F) which is ~20 times higher than those of the preindustrial period. From the HgAR profile, the anthropogenic Hg accumulated since 6 ka in these sediments is 4.0 mg m^{-2} compared to 8.5 during the S1 period.

5.6. Comparison of Hg dynamics between Eastern and Western Mediterranean

A comparison between Hg deposition, vertical transfer, and bottom accumulation between eastern and western Mediterranean abyssal plains is proposed in Fig. 6. The overall average Hg concentration of settling particles collected in the eastern Mediterranean was twice the one of those measured in the western Mediterranean during the same period (Cossa et al., 2021), whereas C_{org} was twice lower. This results in mean annual Hg:C_{org} molar ratios (Table 1) being 3-5 times higher than their equivalent measured in the western Mediterranean basin. In other words, the POM is enriched in Hg in the ultra-oligotrophic eastern Mediterranean. The complex relationship between Hg and C_{org} testifies to the multiplicity of the POM and Hg sources. Hg originates from atmospheric and terrigenous sources, whereas POM mainly comes from *in situ* productivity in the mixed layer and lateral advection of terrigenous sources. The atmospheric Hg deposition consists of aerosol depositions (including Saharan dust and Hg-contaminated aerosols from Europe) and the gaseous exchange, which are removed from the water of the mixed layer by the biological pump and the embedding with marine snow. In this scavenging process, the Hg:C_{org} ratio of the marine OM is limited by the amount of Hg deposited at the sea surface. On the other hand, the lateral advection of Hg-rich terrigenous OM (with high Hg:C_{org} ratios due to anthropogenic inputs from riverine, erosion, and catchment sources) is conveyed from the Adriatic to the deep waters by the vertical convection (Manca et al., 2002). Broadly speaking, Hg is carried by OM but the Hg:C_{org} ratios vary depending on the origin of the OM (marine vs terrigenous) and their anthropogenic components. To sum up, the decrease in Hg flux from surface to bottom

waters of the western basin is due to terrestrial contributions (anthropogenic aerosols and fluvial contributions) scavenged by the biological pump and combined with OM degradation below the upper layer where a part of Hg is involved in the microbiological loop to form mobile species such as Hg^0 and MeHg. In contrast, in the eastern basin, where Hg flux tends to increase with depth, the main Hg inputs are due to Saharan aerosols ballasting the low planktonic matter and the resuspension of sediments from the continental margin. As a result, the vertical Hg transfer at mid-depth and near the bottom is not different between the eastern and the western basins ($p<0.01$, t-tests). The slightly lower Hg fluxes measured in the bottom trap than in surficial sediments observed in the eastern basin, but more marked in the western basin, probably reflect the recent decrease in anthropogenic Hg emissions around the Mediterranean basin (Cossa et al., 2022). This trend is more clearly observed in the western basin, which is more subject to the influence of anthropogenic inputs, than in the eastern basin.

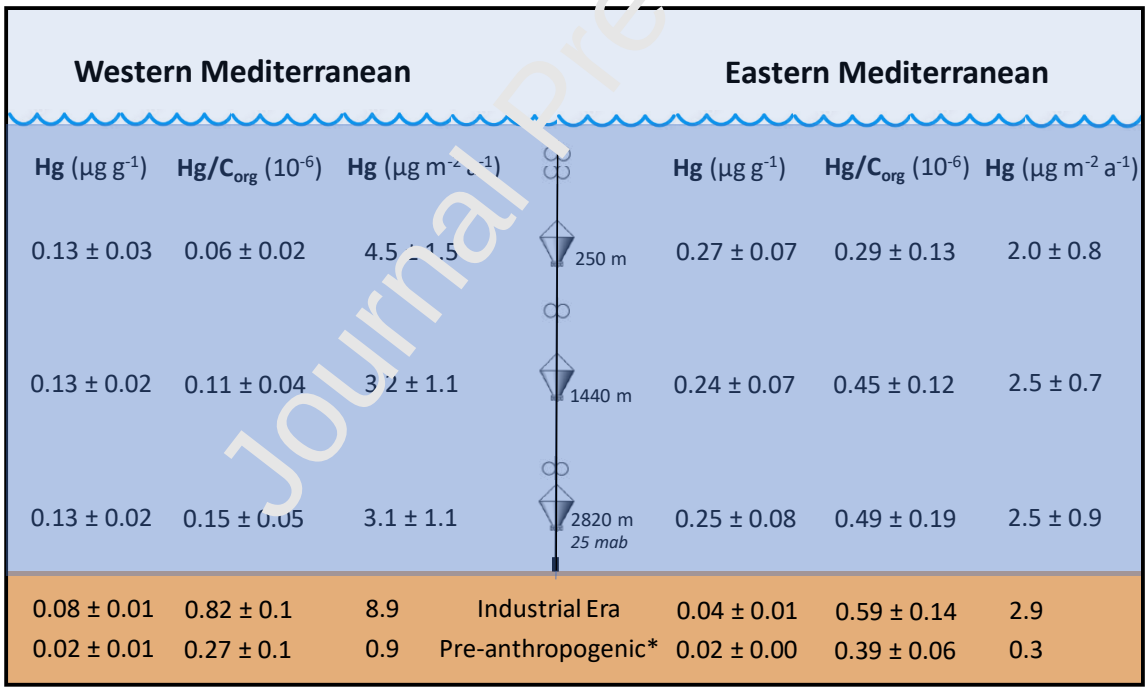

Figure 6. *Mercury (Hg) concentrations and fluxes in the eastern Mediterranean (Ionian abyssal plain) and western Mediterranean (Balearic abyssal plain). Data for the western Mediterranean are from Cossa et al. (2021). (mab) meter above the bottom. * Refers to the pre-anthropogenic period, i.e., before 3 ka cal BP for the western basin and before 6 ka cal BP for the eastern basin excluding Sapropel S1.*

6. Conclusions

This work represents the first direct estimation of the Hg transport through the water column and sedimentary accumulation in the deepest part of the eastern Mediterranean Sea. From the data acquired by sediment traps, mean annual Hg fluxes (May 2001-April 2002) of 2.0, 2.5, and 2.5 μg m^{-2} a^{-1} have been calculated for depths of 250, 1440, and 2820 m (~25 mab), respectively. These Hg flux values are in the same order of magnitude as those estimated for the Mediterranean using the ^{230}Th method (~3 μg m^{-2} a^{-1} see figure 8c in Hayes et al., 2021), slightly lower than those calculated for the western Mediterranean Basin (4.5, 3.2, and 3.1 μg m^{-2} a^{-1}) at equivalent depths (Cossa et al., 2021), and ten times lower than those obtained in sediment trap moored close to the Mediterranean continental margin (Ligurian Sea), i.e., 30 μg m^{-2} a^{-1} (Heimbürger et al., 2012). The highest rates of Hg deposition on the entire water column occur in spring associated with a marine snow consortium composed of Saharan dust and plankton detritus. In other seasons lateral advection of Hg-rich continental sediment occurs below the mixed layer; the convection of Hg-contaminated riverine and coastal sediments is the most probable source for this input.

The HgAR in the Ionian Sea sediments are characterized by the increasing Hg emissions during the Industrial Era and also reflect their changes in the Holocene period. We estimate the pre-anthropogenic HgARs ~0.3 μg m^2 a^{-1}, and the fluxes in the last 150 years around 2.9 μg m^2 a^{-1}; during the Roman period, HgARs have reached ~0.9 μg m^2 a^{-1}. During the Sapropel S1 period, in the mid-Holocene, the Hg fluxes would have been up to 6.4 μg m^2 a^{-1}, as a result of the intensity of the Hg removal by the biological pump and the organic matter preservation in low oxygen environments, along with high inputs of Hg-rich terrigenous matter and a possible restricted Hg recycling in the atmosphere because of the higher stratification of the water column which would have limited the Hg reduction and its reinjection in the atmosphere. Finally, MeHg distribution in the sediment core is a function of the abundance of inorganic Hg and its accumulation in the sediment derives in part from external inputs, but Hg methylation in the transient suboxic conditions of the sapropel is suggested.

Acknowledgment:

This work was supported financially by the European Community in the framework of the ADIOS MAST program (EVK3-CT-2000-00035, Atmospheric deposition, and impact of pollutants on the open Mediterranean Sea). We would also like to thank Pascale Occhipinti and Laurent Nectoux (INERIS) and Bernard Averty (IFREMER) for the Hg and MeHg analyses. Thank are also due to Christophe Migon for his helpful discussion during the redaction of this paper.

Data availability

All the data are given in Suppl. Tables SI.1 and SI.2.

Declaration of interests

☐The authors declare that they have no known competing financial interests or personal relationships that could have appeared to influence the work reported in this paper.

☒The authors declare the following financial interests/personal relationships which may be considered as potential competing interests:

Cossa Daniel reports financial support was provided by IFREMER Atlantic Center.

References

ADIOS, 2004. Atmospheric deposition and Impact of Pollutants, key elements, and nutrients on the open Mediterranean Sea. Final Report, Section 6: detailed report related to overall project duration. 93p. European Communities. Contract number: EVK3-CT-2000-00035. Coordinator: S. Heussner (CNRS, France).

Amos, H.M., Jacob, D.J., Kocman, D., Horowitz, H.M., Zhang, Y., Dutkiewicz, S., Horvat, M., Corbitt, E.S., Krabbenhoft, D.P., Sunderland, E.M., 2014. Global Biogeochemical Implications of Mercury Discharges from Rivers and Sediment Burial. Environ. Sci. Technol., 16, 9514-952. https://doi.org/10.1021/es502134t

Angelidis, M.O., Radakovitch, O., Veron, A., Aloupi, M., Heussner, S., Price, B., 2011. Anthropogenic metal contamination and sapropel imprints in deep Mediterranean sediments. Mar. Pollut. Bull. 62, 1041-1052. https://doi.org/10.1016/j.marpolbul.2011.02.030

Aksentov, K.I., Sattarova, V.V., 2020. Mercury geochemistry of deep-sea sediment cores from the Kuril area, northwest Pacific. Progr. Oceanogr. 180, 102235. https://doi.org/10.1016/j.pocean.2019.102235

Ariztegui, D., Asioli, A., Lowe, J. J., Trincardi, F., Vigliotti, L., Tamburini, F., Chondrogianni, C., Accorsi, C.A., Bandini Mazzanti, M., Mercuri, A.M., van der Kaars, S., McKenzie, J.A., Oldfield, F. (2000). Palaeoclimate and the formation of sapropel S1: inferences from Late Quaternary lacustrine and marine sequences in the central Mediterranean region. Palaeogeogr. Palaeoclimatol. Palaeoecol. 158 (3-4), 215–240. https://doi.org/10.1016/s0031-0182(00)00051-1

Bacon, M.P., 1984. Glacial to interglacial changes in carbonate and clay sedimentation in the Atlantic Ocean estimated from ^{230}Th measurements. Chem. Geol. 46, 97–111. https;//doi.org/10.1016/0009-2541(84)90183-9

Bailey, N., 2021. Saharan Dust as a Mercury Transport Vector. M.Sc. thesis, Department of Environment and Geography. University of Manitoba, Winnipeg, Canada. https://mspace.lib.umanitoba.ca/bitstream/handle/1993/35944/Bailey_Neal.pdf?sequence=1&isAllowed=y

Berline, L., Doglioli, A.M., Petrenko, A., Barrillon, S., Espinasse, B., Le Moigne, F.A. C., Simon-Bot, F., Thyssen, M., Carlotti, F. 2021. Long-distance particle transport to the central Ionian Sea. Biogeosciences 18, 6377–6392. https://doi.org/10.5194/bg-18-6377-2021.

Böttcher, M.E., Rinna, J., Warning, B., Wehausen, R., Howell, M.W., Schnetger, B., Stein, R., Brumsack, H.J., Rullkotter, J., 2003. Geochemistry of sediments from the connection between the western and the eastern Mediterranean Sea (Strait of Sicily, ODP Site 963). Palaeogeogr. Palaeoclimatol. Palaeoecol. 190, 165–194. http://dx.doi.org/10.1016/S0031-0182(02)00604-1

Bouloubassi, I., Rullkotter, J., Meyers, P.A., 1999. Origin and transformation of organic matter in Pliocene-Pleistocene Mediterranean sapropels: organic geochemical evidence

reviewed. Mar. Geol. 153, 177–197. https://doi.org/10.1016/S0025-3227%2898%2900082-6

Bravo, A.G., Cosio, C., 2020. Biotic formation of methylmercury: A bio–physico–chemical conundrum. Limnol. Oceanogr. 65, 1010-1027. https://doi.org/10.1002/lno.11366

Calvert, S.E., Nielsen, B., Fontugne, M.R., 1992. Evidence from nitrogen isotope ratios for enhanced productivity during formation of eastern Mediterranean sapropels. Nature 359, 223–225. https://doi.org/10.1038/359223a0

Castagnoli, G.C., Bonino, G., Caprioglio, F., Provenzale, A., Serio, M., Guang-Mei, Z. 1990. The carbonate profile of two recent Ionian Sea cores: Evidence that the sedimentation rate is constant over the last millennia. Geophys. Res. Lett. 17 (11), 1937–1940. https://doi.org/10.1029/gl017i011p01937

Cossa, D., Coquery, M., 2005. The Mediterranean mercury anomaly: a geochemical or a biological issue. pp 177-208. In: The Mediterranean Sea. Handbook of Environmental Chemistry, Vol. 5. Saliot, A. editor. Springer, 413 p. ISSN 1433-6863. https://hal.inrae.fr/hal-02587234

Cossa, D., Garnier, C., Buscail, R., Elbaz-Poulichet, F., Mikac, N., Patel-Sorrentino, N., Tessier, E., Rigaud, S., Lenoble, V., Gobeil, C., 2014. A Michaelis-Menten type equation for describing methylmercury dependence on inorganic mercury in aquatic sediments. Biogeochemistry 119, 35-43. http://dx.doi.org/10.1007/s10533-013-9924-3

Cossa, D., Mucci, A., Guédron, S., Coquery, M., Radakovich, O., Escoube, R., Campillo, S., Heussner, S., 2021. Mercury accumulation in the sediment of the Western Mediterranean abyssal plain: A reliable archive of the late Holocene. Geochim. Cosmochim. Acta 309, 1-15. https://doi.org/10.1016/j.gca.2021.06.014

Cossa, D., Knoery, J., Bănaru, D., Harmelin-Vivien, M., Sonke, J. E., Hedgecock, I. M., Bravo, A. G., Rosati, G., Canu, D., Horvat, M., Sprovieri, F., Pirrone, N., Heimbürger-Boavida, L.-E., 2022. Mediterranean Mercury Assessment 2022: An Updated Budget, Health Consequences, and Research Perspectives. Environ. Sci. Technol. 56, 3840-3862. http://doi.org/10.1021/acs.est.1c03044

Crusius, J., Thomson, J., 2003. Mobility of authigenic rhenium, silver, and selenium during postdepositional oxidation in marine sediments. Geochim. Cosmochim. Acta 67 (2), 265-273. http://dx.doi.org/10.1016/S0016-7037(02)01075-X

De Lange, G.J., Middelburg, J.J., Pruysers, P.A., 1989. Middle and Late Quaternary depositional sequences and cycles in the eastern Mediterranean. Sedimentology 36 (1), 151–156. https//doi.org/10.1111/j.1365-3091.1989.tb00827.x

De Lange, G.J., Thomson, J., Reitz, A., Slomp, C.P., Speranza Principato, M., Erba, E., Corselli, C., 2008. Synchronous basin-wide formation and redox-controlled preservation of a Mediterranean sapropel. Nat. Geosci. 1, 606-610. https://doi.org/10.1038/ngeo283

Droghini, E., Annibaldi, A., Prezioso, E., Tramontana, M., Frapiccini, E., De Marco, R., Illuminati, S., Truzzi, C., Spagnoli, F., 2019. Mercury Content in Central and Southern Adriatic Sea Sediments in Relation to Seafloor Geochemistry and Sedimentology. Molecules 2019, 24, 4467. https://doi.org/10.3390/molecules24244467

Elbaz-Poulichet, F., Dezileau, L., Freydier, R., Cossa, D., Sabatier, P., 2011. A 3500-year record of Hg and Pb contamination in a Mediterranean sedimentary archive (the Pierre Blanche Lagoon, France). Environ. Sci. Technol. 45, 8642–8647. https://doi.org/10.1021/es2004599

Elbaz-Poulichet, F., Guédron, S., Develle A.-L., Freydier, R., Perrot, V., Rossi, M., Piot, C., Delpoux, S., Sabatier, P., 2020. A 10,000-year record of trace metal and metalloid (Cu, Hg, Sb, Pb) deposition in a western Alpine lake (Lake Robert, France): Deciphering local and regional mining contamination. Quat. Sci. Rev. 228, https://doi.org/10.1016/j.quascirev.2019.106076.

EPA, 2007. Method 7473. Mercury in Solids and Solutions by Thermal Decomposition, Amalgamation, and Atomic Absorption Spectrophotometry (17 pp). https://www.epa.gov/sites/production/files/2015-12/documents/7473.pdf.

Eurachem/Citac, 2000. Quantifying uncertainty in analytical measurement. Ellison, S.L.R. & Williams, A. editors. Tech. Rep. Guide CG4, EURACHEM/CITEC, EURACHEM/CITAC Guide. Third edition. https://www.eurachem.org/images/stories/Guides/pdf/QUAM2012_P1.pdf

Faganeli, J., Pezdic, J., Ogorelec, B., Mišič, M., Najdek, M., 1994. The origin of sedimentary organic matter in the Adriatic. Cont. Shelf. Res. 14 (4), 365-384. https://doi.org/10.1016/0278-4343(94)90024-8

Feyte, S., Tessier, A., Gobeil, C., Cossa, D., 2010. In situ adsorption of mercury, methylmercury and other elements by iron oxyhydroxides and associated organic matter in lake sediments. Appl. Geochem. 25, 984–995. http://doi.org/10.1016/j.apgeochem.2010.04.005

Figueiredo, N., Serralheiro, M.L., Canario, J., Duarte, A., Hintelmann, H., Carvalho, C., 2018. Evidence of Mercury Methylation and Demethylation by the Estuarine Microbial Communities Obtained in Stable Hg Isotope Studies. Environ. Res. Public Health 15, 2141. https://doi.org/10.3390/ijerph15102141

Filippidi, A., De Lange, G.J., 2019. Eastern Mediterranean deep water formation during sapropel S1: A reconstruction using geochemical records along a bathymetric transect in the Adriatic outflow region. Paleoceanogr. Paleoclimatology 34 (3), 409–429. https://doi.org/10.1029/2018PA003459

Fitzgerald, W.F., Engstrom, D.R., Mason, R.P., Nater, E.A., 1998. The case for atmospheric mercury contamination in remote areas. Environ. Sci. Technol. 32 (1), 1-7. https://doi.org/10.1021/es970284w

Fitzgerald, W.F., Lamborg, C.H., Hammerschmidt, C.R., 2007. Marine Biogeochemical Cycle. Chem. Rev. 107 (2), 641-662. https://doi.org/10.1021/cr050353m

Frieling, J., Mather, T.A., März, C., Jenkyns, H.C., Hennekam, R., Reichart, G.-J., Slomp, C.P., van Helmond, N.A.G.M., 2023. Effects of redox variability and early diagenesis on marine sedimentary Hg records. Geochim. Cosmochim. Acta 351, 78-95. https://doi.org/10.1016/j.gca.2023.04.015

Gallisai, R., Peters, F., Volpe, G., Basart, S., Baldasano, J.M., 2014. Saharan Dust Deposition May Affect Phytoplankton Growth in the Mediterranean Sea at Ecological Time Scales. PLoS ONE 9 (10), e110762. https://doi.org/10.1371/journal.pone.011076

Garcia-Orellana, J., Pates, J.M., Masqué, P., Bruach, J., Sanchez-Cabeza, J., 2009. Distribution of artificial radionuclides in deep sediments of the Mediterranean Sea. Sci. Total Environ. 407, 887-898. https://doi.org/10.1016/j.scitotenv.2008.09.018

Gehrke, G.E., Blum, J.D., Meyers, P.A., 2009. The geochemical behavior and isotopic composition of Hg in a mid-Pleistocene western Mediterranean sapropel. Geochim. Cosmochim. Acta 73, 1651–1665. http://dx.doi.org/10.1016/j.gca.2008.12.012

Georgopoulos, D., Anagnostou, C., Zervakis, V., Karageorgis, A., Stavrakakis, S., Kaberi, A.P., Papadopoulos, V., Kioroglou, S., Papadopoulos, A., Perivoliotis, L., 2002. The "ADIOS" project in the eastern Mediterranean Sea. Hydrology and dynamics, particulate matter and down fluxes. International Conference on Oceanography of the Eastern Mediterranean and Black Sea: similarities and differences of two interconnected basins (Ankara, Turkey). https://www.researchgate.net/publication/263656088

Gobeil, C., Cossa, D., 1993. Mercury in the sediments and sediment pore waters in the Laurentian Trough. Can. J. Fish. Aquat. Sci. 50, 1794-1800. https://doi.org/10.1139/f93-201

Gobeil, C., MacDonald, R., Smith, J.N. 1999. Mercury profiles in sediments of the Arctic Ocean basins. Environ. Sci. Technol. 33, 4194-4198 https://doi.org/10.1021/es990471p

Grant, K., Grimm, R., Mikolajewicz, U., Marino, G., Ziegler, M., Rohling, E., 2016. The timing of Mediterranean sapropel deposition relative to insolation, sea-level and African monsoon changes. Quat. Sci. Rev. 140, 125-141. https://doi.org/10.1016/j.quascirev. 2016.03.026

Guerzoni, S., Molinaroli, E., Chester, R., 1997. Saharan dust inputs to the western Mediterranean Sea: depositional patterns, geochemistry and sedimentological implications. Deep-Sea Res. II, 44, 631–654. https://doi.org/10.1016/S0967-0645(96)00096-3

Guerzoni, S., Chester, R., Dulac, F., Moulin, C., Herut, B., Loÿe-Pilot, M.-D., Measures, C., Migon, C., Molinaroli, E., Rossini, P., Saydam, C., Soudine, A., Ziveri, P., 1999. The role of atmospheric deposition in the biogeochemistry of the Mediterranean Sea. Progr. Oceanogr. 44 (1-3), 147-190. https://doi.org/ 10.1016/S0079-6611(99)00024-5

Guieu, C., Schevchenko, V., 2015. Dust in the Ocean. Encyclopedia of Marine Geosciences, 1-8. Springer Science+Business Media, Dordrecht.https://doi.org/10.1007/978-94-007-6644-0-56-3.

Hamilton, E.L., 1976. Variations of density and porosity with depth in deep-sea sediments. J. Sediment. Res. 40 (2), 280-230. https://doi.org/10.1306/212F6F3C-2B24-11D7-8648000102C1865D

Hayes, C.T., Costa, K.M., Anderson, R.F., Calvo, E., Chase, Z., Demina, L.L., et al., 2021. Global ocean sediment composition and burial flux in the deep sea. Glob. Biogeochem. Cycles 35, e2020GB006769. https://doi.org/10.1029/2020GB006769

Heimbürger, L.E., Cossa, D., Thibodeau, B., Khripounoff, A., Mas, V., Chiffoleau, J.-F., Schmidt, S., Migon, C., 2012. Natural and anthropogenic trace metals in sediments of the Ligurian Sea (Northwestern Mediterranean). Chem. Geol. 291, 141-151. https://doi.org/10.1016/j.chemgeo.2011.10.011

Heussner, S., Ratti, C., Carbonne, J., 1990. The PPS3 sediment trap and trap sample processing techniques used during the ECOMARGE experiment. Cont. Shelf Res. 10, 943-958. https://doi.org/10.1016/0278-4343(90)90069-X

Jiskra, M., Heimbürger-Boavida, L.-E., Desgranges, M.-M., Petrova, M.V., Dufour, A., Ferreira-Araujo, B., Masbou, J., Chmeleff, J., Thyssen, M., Point, D., Sonke, J.E., 2021. Mercury stable isotopes constrain atmospheric sources to the ocean. Nature 597, 662. https://doi.org/10.1038/s41586-021-03859-8

Kandler, K., Benker, U., Bundke, N., Cuevas, E., Ebert, M., Knippertz, P., Rodriguez, S., Schütz, L., Weinbruch, S., 2007. Chemical composition and complex refractive index of Saharan Mineral Dust at Izaña, Tenerife (Spain) derived by electron microscopy. Atmos. Environ. 41, 37, 8058-8074. https://doi.org/10.1016/j.atmosenv.2007.06.047

Kostka, J.E., Luther, G.W., 1994. Partitioning and speciation of solid phase iron in saltmarsh sediments. Geochim. Cosmochim. Acta 58, 1701–1710. https://doi.org/10.1016/0016-7037(94)90531-2

Kotnik, J., Horvat, M., Ogrinc, N., Fajon, V., Zizek, D., Cossa, D., Sprovieri, F., Pirrone, N., 2015. Mercury speciation in the Adriatic Sea. Mar. Pollut. Bull. 96 (1/2), 136–148. https://doi.org/10.1016/j.marpolbul.2015.05.037

Lamborg, C., Bowman, K., Hammerschmidt, C., Gilmour, C., Munson, K., Selin, N., Tseng, C.-M., 2014. Mercury in the anthropocene ocean. Oceanography 27 (1), 76–87. https://doi.org/10.5670/oceanog.2014.11

Lamborg, C.H., Hammerschmidt, C.R., Bowman, K.L., 2016. An examination of the role of particles in oceanic mercury cycling. Phil. Trans. R. Soc. A 374, 20150297. https://doi.org/10.1098/rsta.2015.0297

Leermakers, M., Galletti, S., De Galan, S., Brion, N., Baeyens, W., 2001. Mercury in the Southern North Sea and Scheldt estuary. Mar. Chem. 75, 229–248. https://doi.org/10.1016/S0304-4203(01)00039-1

Lim, D., Kim, J., Xu, Z.K., Jeong, K., Jung, H., 2017. New evidence for Kuroshio inflow and deepwater circulation in the Okinawa Trough, East China Sea: Sedimentary mercury variations over the last 20kyr. Paleoceanography 32, 571–579. https://doi.org/10.1002/2017PA003116

Manca, B.B., Kovaĉević, V., Gaĉić, M, Viezzoli, D., 2002. Dense water formation in the Southern Adriatic Sea and spreading into the Ionian Sea in the period 1997-1999. J. Mar. Systems 33-34, 133-154. https://doi.org/10.1016/S0924-7963(02)00056-8

Margaritelli G., Cacho I., Català A., Barra M., Belluci L.G., Lubritto C., Rettori R., Lirer F. 2020. Persistent warm Mediterranean surface waters during the Roman period. Sci. Rep. 10**,** 10431. https://doi.org/10.1038/s41598-020-67281-2

Mason, R.P., Choi, A.L., Fitzgerald, W.F., Hammerschmidt, C.R., Lamborg, C.H., Soerensen, A.L., Sunderland, E.M., 2012. Mercury biogeochemical cycling in the ocean and policy implications. Environ. Res. 119, 101-117. https://doi.org/10.1016/j.envres.2012.03.013

Mercone, D., Thomson, J., Croudace, I.W., Troelstra, S.R., 1999. A coupled natural immobilization mechanism for mercury and selenium in deep-sea sediments Geochim. Cosmochim. Acta 63, 1481-1488. https://doi.org/10.1016/S0016-7037(99)00063-0

Mikac, N., Niessen, S., Ouddane, B., Fisher J.-C., 2000. Effects of acid volatile sulfides on the use of hydrochloric acid for determining solid-phase associations of mercury in sediments. Environ. Sci. Technol. 34, 1871–1876. https://doi.org/10.1021/es990477e

Moulin, C., Lambert, C.E., Dayan, U., Masson, V., Ramonet, M., Bousquet, P., Legrand, M., Balkanski, Y.J., Guelle, W., Marticorena, B., Bergametti, G., Dulac, F., 1998. Satellite climatology of African dust transport in the Mediterranean atmosphere. J. Geophys. Res. Atmos. 103, 13137–13144. https://doi.org/10.1029/98JD00171

Munson, K.M., Lamborg, C.H., Swarr, G.J., Saito, M.A., 2015. Mercury species concentrations and fluxes in the Central Tropical Pacific Ocean. Glob. Biogeochem. Cycles 29, 656–676. https://doi.org/10.1002/2015GB005120

Murat, A., Got, H., 2000. Organic carbon variations of the eastern Mediterranean Holocene sapropel: a key for understanding formation processes. Palaeogeogr. Palaeoclimatol. Palaeoecol. 158, 241–257. https://doi.org/10.1016/S0031-0182(00)00052-3

Nikitas, A., Triantaphyllou, M.V., Rousakis, G., Panagiotopoulos, I., Pasadakis, N., Hatzianestis, I., Gogou, A., 2021. Pre-Messinian Deposits of the Mediterranean Ridge: Biostratigraphic and Geochemical Evidence from the Olimpi Mud Volcano Field. Water, 13, 1367. https://doi.org/10.3390/w13101367

Ogrinc, N., Monperrus, M., Kotnik, J., Fajon, V., Vidimova, K., Amouroux, D., Kocman, D., Tessier, E., Žižek, S., Horvat, M., 2007. Distribution of mercury and methylmercury in deep-sea surficial sediments of the Mediterranean Sea. Mar. Chem. 107 (1), 31–48. http://dx.doi.org/10.1016/j.marchem.2007.01.019

Ogrinc, N., Hintelmann, H., Kotnik, J., Horvat, M., Pirrone, N., 2019. Sources of mercury in deep-sea sediments of the Mediterranean Sea as revealed by mercury stable isotopes. Sci. Rep. 9, 11626. https://doi.org/10.1038/s41598-019-48061-z

Outridge, P.M., Sanei, H., Stern, G.A., Hamilton, P.B., Goodarzi, F., 2007. Evidence for Control of Mercury Accumulation Rates in Canadian High Arctic Lake Sediments by Variations of Aquatic Primary Productivity. Environ. Sci. Technol. 41, 5259-5265. https://doi.org/10.1021/es070408x

Outridge, P.M., Mason, R.P., Wang, F., Guerrero, S., Heimbürger-Boavida, L.-E., 2018. Updated Global and Oceanic Mercury Budgets for the United Nations Global Mercury Assessment 2018. Environ. Sci. Technol. 52, 12968–12977. https://doi.org/10.1021/acs.est.8b01246

Pedrosa-Pàmies, R., Sanchez-Vidal, A., Canals, M., Lampadariou, N., Velaoras, D., Gogou, A., Parinos, C., Calafat, A., 2016. Enhanced carbon export to the abyssal depths driven by atmosphere dynamics. Geophys. Res. Lett. 43, 8626-8636. https://doi.org/10.1002/2016GL069781

Pedrosa-Pamies, R., Parinos, C., Sanchez-Vidal, A., Calafat, A., Canals, M., Velaoras, D., Mihalopoulos, N., Kanakidou, M., Lampadariou, N., Gogou, A., 2021. Atmospheric and Oceanographic Forcing Impact Particle Flux Composition and Carbon Sequestration in the Eastern Mediterranean Sea: A Three-Year Time-Series Study in the Deep Ierapetra Basin. Front. Earth Sci. 9, 591948. https://doi.org/10.3389/feart.2021.591948

Powley, H.P., Van Cappellen, P., Krom, M.D., 2017. Nutrient Cycling in the Mediterranean Sea: The Key to Understanding How the Unique Marine Ecosystem Functions and Responds to Anthropogenic Pressures, Mediterranean Identities - Environment, Society, Culture, Borna Fuerst-Bjelis, IntechOpen. hppts://doi.org/10.5772/intechopen.70878. https://www.intechopen.com/chapters/57227.

Pruysers, P.A., De Lange, G.J., Middelburg, J.J., 1991. Geochemistry of eastern Mediterranean sediments: Primary sediment composition and diagenetic alteration. Mar. Geol. 100, 137–154. https://doi.org/10.1016/0025-3227(91)90230-2

Regnell, O., Watras, C.J., 2019. Microbial mercury methylation in aquatic environments: A critical review of published field and laboratory studies. Environ. Sci. Technol. 53, 4–19. https://doi.org/10.1021/acs.est.8b02709

Reimer, P.J., Austin, W.E.N., Bard, E., Bayliss, A., Blackwell, P.G., Bronk Ramsey, C., Butzin, M., Cheng, H., Edwards, R.L., Friedrich, M., Grootes, P.M., Guilderson, T.P., Hajdas, I., Heaton, T.J., Hogg, A.G., Hughen, K.A., Kromer, B., Manning, S.W., Muscheler, R., Palmer, J.G., Pearson, C., van der Plicht, J., Reimer, R.W., Richards, D.A., Scott, E.M., Southon, J.R., Turney, C.S.M., Wacker, L., Adolphi, F., Büntgen, U., Capano, M., Fahrni, S.M., Fogtmann-Schulz, A., Friedrich, R., Köhler, P., Kudsk, S., Miyake, F., Olsen, J., Reinig, F., Sakamoto, M., Sookdeo, A., Talamo, S., 2020. The IntCal20 Northern Hemisphere Radiocarbon Age Calibration Curve (0–55 cal kBP). Radiocarbon 62, 725-757. https://doi.org/10.1017/RDC.2020.41

Rohling, E., Marino, G., Grant, K., 2015. Mediterranean climate and oceanography, and the periodic development of anoxic events (sapropels). Earth-Sci. Rev. 143, 62-97. https://doi.org/10.1016/j.earscirev.2015.01.008

Rutten, A., De Lange, G.J., Ziveri, P., Thomson, J., van Santvoort, P.J.M., Colley, S., Corselli, C., 2000. Recent terrestrial and carbonate fluxes in the pelagic eastern Mediterranean; a comparison between sediment trap and surface sediment. Paleogeogr. Paleoclimatol. Paleoecol. 158, 197–213. http://dx.doi.org/10.1016/S0031-0182(00)00050-X

Rydberg, J., Gälman, V., Renberg, I., Bindler, R., 2008. Assessing the Stability of Mercury and Methylmercury in a varved Lake Sediment Deposit. Environ. Sci. Technol. 42, 4391-4396. https://doi.org/10.1021/es7031955

Sanei, H., Outridge, P.M., Oguri, K., Stern, G.A., Thamdrup, B., Wenzhöfer, F., Wang, F., Glud, R.N., 2021. High mercury accumulation in deep-ocean hadal sediments. Sci. Rep. 11, 10970. https://doi.org/10.1038/s41598-021-90459-1

Sciarra, R., Volpe, G., Santoleri, R., 2004. SeaWiFS observations of Saharan dust events over the Mediterranean Sea. Remote Sensing of the Ocean and Sea Ice 2003. C. R. Bostater, Jr., R. Santoleri editors, Proceedings of SPIE, Vol. 5233, SPIE, Bellingham, WA, USA. https://doi.org/10.1117/12.516641

Siani, G., Paterne, M., Arnold, M., Bard, E., Métivier, B., Tisnerat, N., Bassinot, F., 2000. Radiocarbon Reservoir Ages in the Mediterranean Sea and Black Sea. Radiocarbon 42, 271-280. https://doi.org/10.1017/S0033822200059075

Skampa, E., Triantaphyllou, M.V., Dimiza, M.D., Gogou, A., Malinverno, E., Stavrakakis, S., Parinos, C., Panagiotopoulos, I.P.? Tselenti, D., Archontikis, O., Baumann, K.-H., 2020. Coccolithophore export in three deep-sea sites of the Aegean and Ionian Seas (Eastern Mediterranean): Biogeographical patterns and biogenic carbonate fluxes. Deep Sea Res. Part II 171, 104690. https://doi.org/10.1016/j.dsr2.2019.104690

Ternon, E., Guieu C., Loyë-Pilot M.-D., Leblond N., Bosc E., Gasser B., Miquel J.-C., Martín, J., 2010. The impact of Saharan dust on the particulate export in the water column of the North Western Mediterranean Sea. Biogeosciences 7, 809–826. https://doi.org/10.5194/bg-7-809-2010

The MerMex Group: Durrieu de Madron, X., Guieu, C., Sempéré, R., Conan, P., Cossa, D. et al., 2011. Marine ecosystems' responses to climatic and anthropogenic forcings in the Mediterranean. Progr. Oceanogr. 91, 97-166. https://doi.org/10.1016/j.pocean.2011.02.003

Thevenon, F., Guédron S., Chiaradia M., Loizeau J.-L., Poté J., 2011 (Pre-) historic changes in natural and anthropogenic heavy metals deposition inferred from two contrasting Swiss Alpine lakes. Quaternary Sci. Rev. 30, 224–233. https://doi.org/10.1016/j.quascirev.2010.10.013

Thomson, J., Higgs, N.C., Wilson, T.R.S., Croudace, I.W., De Lange, G.J., Van Santvoort, P.J.M., 1995. Redistribution and geochemical behaviour of redox-sensitive elements around S1, the most recent eastern Mediterranean sapropel. Geochim. Cosmochim. Acta 59, 3487–3501. https://doi.org/10.1016/0016-7037(95)00232-O

van Kemenade, Z.R., Cutmore, A., Hennekam, R., Hopmans, E.C., van der Meer, M.T., Mojtahid, M., Jorissen, F.J., Bale, N.J., Reichart, G.-J., Damsté, J.S.S., 2023. Marine nitrogen cycling dynamics under altering redox conditions: insights from deposition of sapropels S1 and the ambiguous S2 in the Eastern Mediterranean Sea. Geochim. Cosmochim. Acta 354, 197-210. https://doi.org/10.1016/j.gca.2023.06.018

Van Santvoort, P.J.M., De Lange, G.J., Thomson, J., Cussen, H., Wilson, T.R.S., Krom, M.D., Ströhle, K., 1996. Active post-depositional oxidation of the most recent sapropel (S1) in sediments of the eastern Mediterranean Sea. Geochim. Cosmochim. Acta 60, 4007–4024. https://doi.org/10.1016/S0016-7037(96)00253-0

Vincent, J., Laurent, B., Losno, R., Bon Nguyen, E., Roullet, P., Sauvage, S., Chevaillier, S., Coddeville, P., Ouboulmane, N., di Sarra, A. G., Tovar-Sánchez, A., Sferlazzo, D., Massanet, A., Triquet, S., Morales Baquero, R., Fornier, M., Coursier, C., Desboeufs, K., Dulac, F., and Bergametti, G., 2016. Variability of mineral dust deposition in the western Mediterranean basin and south-east of France. Atmos. Chem. Phys. 16, 8749–8766. https://doi.org/10.5194/acp-16-8749-2016

Wehausen, R., Brumsack, H.J., 2000. Chemical cycles in Pliocene sapropel-bearing and sapropel-barren eastern Mediterranean sediments. Paleogeogr. Paleoclimatol. Paleoecol. 158 (3-4), 325-352. http://dx.doi.org/10.1016/S0031-0182(00)00057-2

Zhang, Y., Jacob, D.J., Dutkiewicz, S., Amos, H.M., Long, M.S., Sunderland, E.M., 2015. Biogeochemical drivers of the fate of riverine mercury discharged to the global and Arctic oceans. Glob. Biogeochem. Cycles 29, 854–864. https://doi.org/10.1002/2015gb005124

Zambardi, T., Sonke, J.E., Toutain, J.P., Sortino, F., Shinohara, H., 2009. Mercury emissions and stable isotopic compositions at Volcano Island (Italy). Earth. Planet. Sci. Lett. 277 (1), 236–243. https://doi.org/10.1016/j.epsl.2008.10.023

Figure captions

Figure 1. Locations of the sampling stations in the Ionian Sea. Sta. EA: boxcore; Sta. EB: sediment trap mooring.

Figure 2. (A) lithogenic fraction, (B) C_{org}, (C) carbonates, and (D) total mass flux in the three sediment traps at Sta. EB during the period May 2001 to April 2002.

Figure 3. (A) Hg concentration in the particulate material collected during the year 2001-2002 in the three sediment traps at Sta. EB. Low Hg concentrations are observed in spring; (B) Hg vs organic carbon (C_{org}) in particulate material collected during the year 2001-2002 in the three sediment traps at Sta. EB. Low $\delta^{13}C$ values, suggesting terrigenous OM, are associated with Hg-rich particles. C_{org} > 6% values may involve a bio-dilution of particulate Hg.

Figure 4. Vertical distributions of C_{org} (A), Ba/Al (B), Mn/Al with Mo/Al (C), Hg (D), MeHg (C), and HgAP (F) in sediment cores EA and EB. The onset, ending, and oxidized part of the sapropel S1 are indicated (see text). The oxidized front is defined by the presence of Mn/Al and Mo/Al peaks.

Figure 5. Methylmercury (MeHg) and manganese (Mn) relationship in the EA sediments. The oxidation front and oxidized sapropel cover the 14-20 cm sediment layer. In this layer, the MeHg vs Mn relationship exhibits an R^2 of 0.96 ($p<0.01$).

Figure 6. Mercury (Hg) concentrations and fluxes in the Eastern Mediterranean (Ionian abyssal plain) and Western Mediterranean (Balearic abyssal plain). Data for the western Mediterranean are from Cossa et al. (2021). (mab) meter above the bottom. * Refers to

the pre-anthropogenic period, i.e., before 3 ka cal BP for the western basin and before 6 ka cal BP for the eastern basin excluding Sapropel S1.

Table captions

Table 1. Mean concentrations (±1SD) of main components of the particles collected in the traps between twice a month May 2001 and April 2002 at Sta. EB. * Mean concentration significantly ($p<0.01$) different from means at 1440 and 2820 m; other differences are non-significant.